frontiers in Mechanical Engineering

ORIGINAL RESEARCH
published: 22 July 2021
doi: 10.3389/fmech.2021.686638

Smoldering and Flaming of Disc Wood Particles Under External Radiation: Autoignition and Size Effect

Supan Wang[1,2], Pengfei Ding[1], Shaorun Lin[2], Junhui Gong[1] and Xinyan Huang[2]**

[1]College of Safety Science and Engineering, Nanjing Tech University, Nanjing, China, [2]Research Centre for Fire Safety Engineering, The Hong Kong Polytechnic University, Kowloon, Hong Kong

Wildfires are global issues that cause severe damages to the society and environment. Wood particles and firebrands are the most common fuels in wildfires, but the size effect on the flaming and smoldering ignitions as well as the subsequent burning behavior is still poorly understood. In this work, a well-controlled experiment was performed to investigate smoldering and flaming ignitions of stationary disc-shaped wood particles with different diameters (25–60 mm) and thicknesses (15–25 mm) under varying radiant heat flux. The ignition difficulty, in terms of the minimum heat flux, increases from smoldering ignition to piloted flaming ignition and then to flaming autoignition. As the sample thickness increases, the minimum heat flux, ignition temperature, and burning duration for flaming autoignition all increase, while the peak burning flux decreases, but they are insensitive to the sample diameter. During ignition and burning processes, the disc particle is deformed due to the interaction between chemical reactions and thermomechanical stresses, especially for smoldering. The characteristic thickness of the smoldering front on wood is also found to be 10–15 mm. This study sheds light on the size effect on the ignition of wood particles by wildfire radiation and helps understand the interaction between flaming and smoldering wildfires.

Keywords: ignition limit, minimum radiation, disc particles, smoldering fire, firebrands

OPEN ACCESS

Edited by:
Naian Liu,
University of Science and Technology of China, China

Reviewed by:
Alexander S. Rattner,
The Pennsylvania State University (PSU), United States
Patrick Jacob Shamberger,
Texas A&M University, United States

****Correspondence:***
Shaorun Lin
flynn.lin@connect.polyu.hk
Xinyan Huang
xy.huang@polyu.edu.hk

Specialty section:
This article was submitted to Thermal and Mass Transport, a section of the journal Frontiers in Mechanical Engineering

Received: *27 March 2021*
Accepted: *22 June 2021*
Published: *22 July 2021*

Citation:
Wang S, Ding P, Lin S, Gong J and Huang X (2021) Smoldering and Flaming of Disc Wood Particles Under External Radiation: Autoignition and Size Effect. Front. Mech. Eng 7:686638. doi: 10.3389/fmech.2021.686638

INTRODUCTION

Driven by the climate change, the Earth ecosystems tend to suffer more frequent wildfires and longer wildfire durations, posing severe threats to the economy, society, and environment, especially in the densely populated wildland–urban interface (WUI) (Liu et al., 2010; Moritz et al., 2014; Toledo et al., 2018; Lin et al., 2019a). Mega-scale wildfires are difficult to predict and control, and they may cause huge casualties and property loss, such as those in California, Australia, and South Europe. Because the spread of a wildfire is a result of a consecutive ignition process (Williams, 1982), it is critical to understand the ignition of wildland fuel particles to predict wildfire development and optimize the emergency response.

The ignition of wildland fuel involves complex physicochemical processes in both the solid and gas phases, and it depends on fuel properties, for example, density, type, moisture, and thermal conductivity (Simms and Law 1967; Wesson et al., 1971; Bilbao et al., 2001), and configurations, for example, size and shape (Saastamoinen et al., 2000; Momeni et al., 2013; Lin et al., 2019a). Small fuel particles, such as shrubs, twigs, bark, and litter layer, constitute a vast majority of wildland fuel loads, so the ignition of small particles is closely related to the wildfire risks and hazards (Moghtaderi et al., 1997; McAllister 2013; Finney et al., 2015; Lin et al., 2019a). The recent debate on the ignition

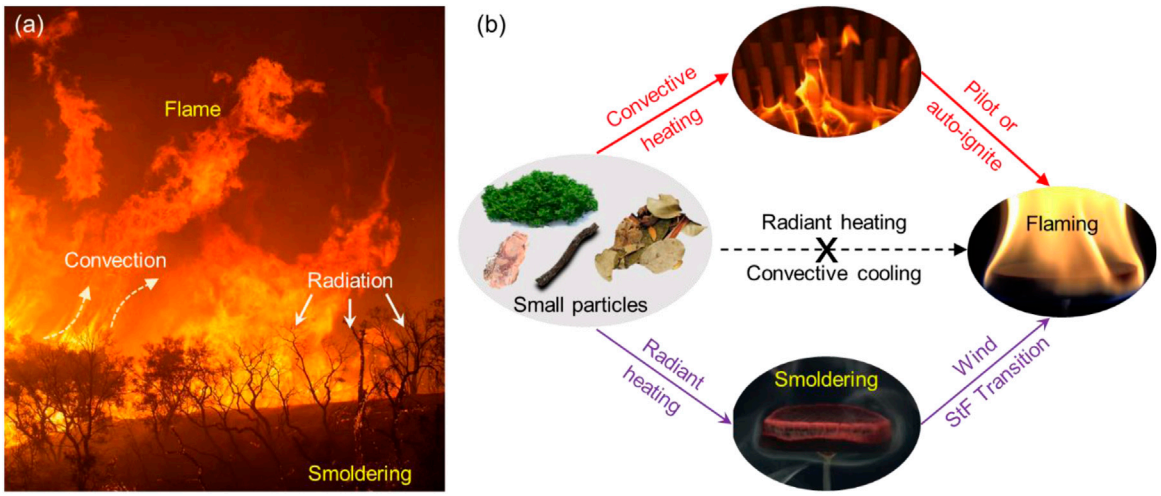

FIGURE 1 | (A) Flaming and smoldering fire of wood particles in wildfires (U.S. Forest Surveys) and **(B)** possible ignition mode of wood particles.

mechanism (Finney et al., 2013, 2015) suggested that direct flame contact played a dominant role in the flaming ignition of fine and small fuel particles, which compensated Rothermel's radiation ignition theory (Rothermel, 1972).

Almost all wildland fuels can sustain both forms of flaming and smoldering wildfires (**Figure 1A**), such as pine needle beds (Wang et al., 2017a), barks and twigs (Sullivan et al., 2018), ground litter layers (Wang et al., 2017b), and underground organic soils (Lin et al., 2019b). Flaming fire is sustained by the oxidation of pyrolysis gases in the gas phase (Quintiere, 2006). Smoldering is dominated by the char oxidation in the solid phase, so it is slow, low-temperature, flameless, and the most persistent (Rein, 2014). The ignition of smoldering does not need a pilot source, so it is also a kind of autoignition or spontaneous ignition. Both flaming and smoldering fire can transition to each other under specific conditions (Santoso et al., 2019; Huang and Gao 2020; Lin et al., 2021). As illustrated in **Figure 1B**, the flame can be piloted by direct contact with a nearby flame (Finney et al., 2015) or autoignited within the hot plume (McAllister et al., 2012; Mcallister and Finney 2017). Also, the flame can be transitioned from the smoldering fire, that is, the smoldering-to-flaming (StF) transition. Compared to piloted flaming ignition, smoldering ignition needs no pilot source. Moreover, the intensified convective cooling, which prevents the flaming ignition under radiation (Finney et al., 2013), can also facilitate and intensify smoldering by increasing the oxygen supply (Wang et al., 2016). In other words, smoldering provides an alternative shortcut for flaming ignition in the absence of direct flame contact, but it needs further verification under specific fuels and environmental conditions.

The shape of wildland fuels may be cubic, cylindrical, spherical, disc-shaped, or irregular (Paulrud and Nilsson 2004; Kuo and Hsi 2005; Lin et al., 2019a). The fuel size also has a wide range, from mm-scale fine leaves and needles (McAllister et al., 2012) to cm-scale small twigs, shrubs, and firebrands (Manzello et al., 2008; Manzello et al., 2020) to dm-scale tree trunks and to m-scale soil layers (Huang and Rein, 2017). Most research literature focused on the flaming and smoldering ignition limits of flat wood samples under external irradiation (Boonmee and Quintiere 2002; Yang et al., 2011). Nevertheless, the effects of fuel shape and size are also important. Harada (2002) pointed out that the sample thickness did not influence the flaming ignition delay time but affected the mass-loss rate. Finney et al. (2015) revealed that for the fine-sized fuel particles, the convective cooling dominated over the radiant heating, whereas the convective heating *via* contact with flames and hot gases controlled the flaming ignition. Lin et al. (2019a) showed the combined effects of fuel size and arrangement on the convective cooling and the piloted flaming ignition under external radiation. Atreya et al. (2017) also pointed out that the nominal dimensions (i.e., size and shape) have a significant effect on the pyrolysis duration and the remaining char mass. To the best of the authors' knowledge, very limited research was available on the smoldering and flaming autoignition and burning behaviors of small wildland fuel particles and the effect of particle size; thus, there is a big knowledge gap.

In this work, the smoldering ignition of disc-shaped hardwood particles is investigated with different sizes (5–60 mm) under an external radiation up to 60 kW/m^2. For comparison, the flaming autoignition experiments are also conducted. The ignition delay time, temperature, minimum heat flux, and burning rate are quantified and analyzed to provide a full picture of wildland fuel ignitability.

EXPERIMENTAL METHOD

Apparatus and Fuel Sample

The schematic diagram of the experimental setup is illustrated in **Figure 2**, and it mainly consists of a radiant panel, a sample holder, and an electric balance. The panel radiator with the dimension of 0.2 m × 0.2 m is made of several resistance heating rods that can generate a uniform radiant heat flux from 0 to 60 kW/m^2 on the top fuel surface 50 mm below. The air temperature above the wood surface is lower, so the

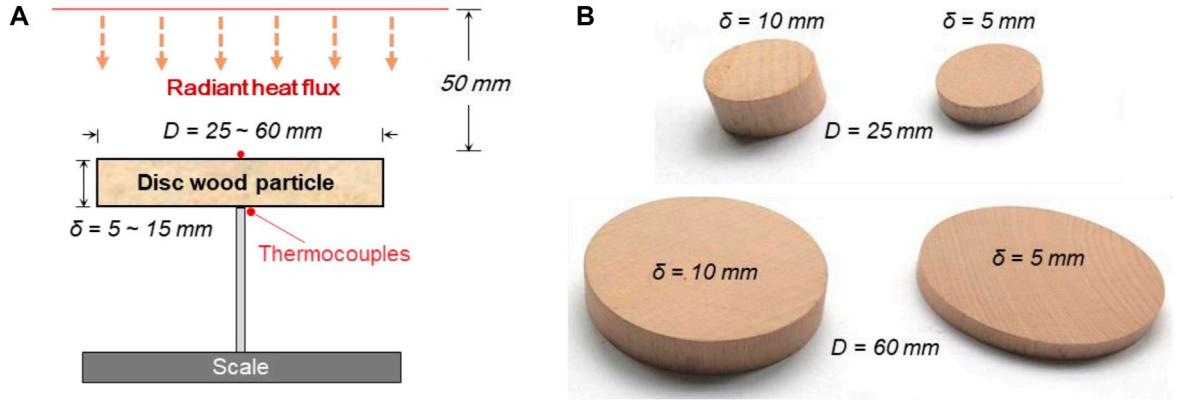

FIGURE 2 | (A) Schematic diagram of the test setup for igniting the disc-shaped wood particle under external radiation, and **(B)** photos of disc-shaped wood particles with different thicknesses and diameters.

air is responsible for cooling the wood surface. The fuel particles tested in the experiment were German beech wood. Referring to the survey of wood particle shapes and sizes in common wildlands (Manzello et al., 2008), nine disc-shaped samples with three diameters (D) of 25, 40, and 60 mm and three thicknesses (δ) of 5, 10, and 15 mm were tested. These wood samples were first oven-dried at 80°C for 8 h and then kept in a dry chamber to control the same initial condition. The initial mass of particle samples ranges from 1.6 to 25.8 g with an uncertainty of 5%, so their dry bulk density was calculated to be 621 ± 21 kg/m^3.

The wood particle was stuck to a 2-mm-thick aluminum rod using high-temperature-resistant adhesive, and then it was spaced for 5 h to form a stable connection. During the experiment, the mass evolution of the particle was measured using the electric balance (Mettler-Toledo XE10002S, resolution: 0.01 g). The upper and lower surface temperatures of the particle were measured using two thin K-type thermocouples (TCs) with a 0.5-mm bead. Because thermocouples might affect the mass measurement, the mass and temperature measurements were conducted separately in repeating tests.

Ignition Protocols

Before testing, the radiant panel was first preheated for 25 min to the prescribed heat flux which was measured and calibrated using a radiometer. Afterward, the irradiation was shielded using an insulation board that allowed the sample to be placed in the right position. Once the insulation shield was removed, the irradiation started to apply to the sample. It should be noted that no pilot source was used for flaming ignition, different from the study by Lin et al. (2019b). The whole heating and burning process was recorded using a front-view video camera (Sony FDR-AX60 at 50 fps). For any given experimental condition, the experiment was repeated 3–6 times to quantify the random uncertainty.

For the flaming autoignition, the ignition delay time ($t_{ig,f}$) could be easily quantified visually when the flame appeared. The minimum radiation for autoignition ($\dot{q}''_{min,f}$) can be obtained by decreasing the incident heat flux until no flame occurs after heating for 10 min. For the smoldering ignition, it was difficult to visually determine the onset of smoldering. Approximately, based on the threshold temperature of char oxidation (Terrei et al., 2019), the characteristic temperature of 350 ± 30°C can be defined as the threshold of smoldering. By reducing the radiation, the minimum value for smoldering ignition ($\dot{q}''_{min,sm}$) was determined when the sample had no mass loss after being fully charred.

RESULTS AND DISCUSSION

Smoldering Ignition and Burning Behaviors

Figure 3A shows an example of the smoldering ignition process and the associated burning behaviors of wood particles with the same diameter of 60 mm and two different thicknesses of 10 and 15 mm, respectively. The original videos can be found in **Supplementary Video S1, 2**. Once exposed to the irradiation, the sample was heated to release some visible smoke. The visible smoke may be the condensed water droplets (like fog) and tar droplets (the condensed pyrolysis gases with a high molecular weight) as they mix with cool air. The intensity of the smoke flow first increased, which may even form the gas jet above the sample surface, and then it gradually decreased near burnout. The flow of air streams was faster near the edge of the surface with a large curvature that can enhance convective heat transfer (Incropera and DeWitt, 1996). Moreover, due to the better oxygen supply, noticeable glowing was always first initiated at the edge, which is a widely observed phenomenon on the solid surface (Huang and Gao, 2020).

During the smoldering ignition and the burning process, complex structural behaviors of wood particles could be observed, and the deformation was more obvious for the disc sample with a larger diameter-to-thickness ratio. As shown in **Figure 3A**, there are mainly two different deformation stages:

i) Bending upward to form a bowl shape. Once exposed to the irradiation, the wood sample started to deform upward and

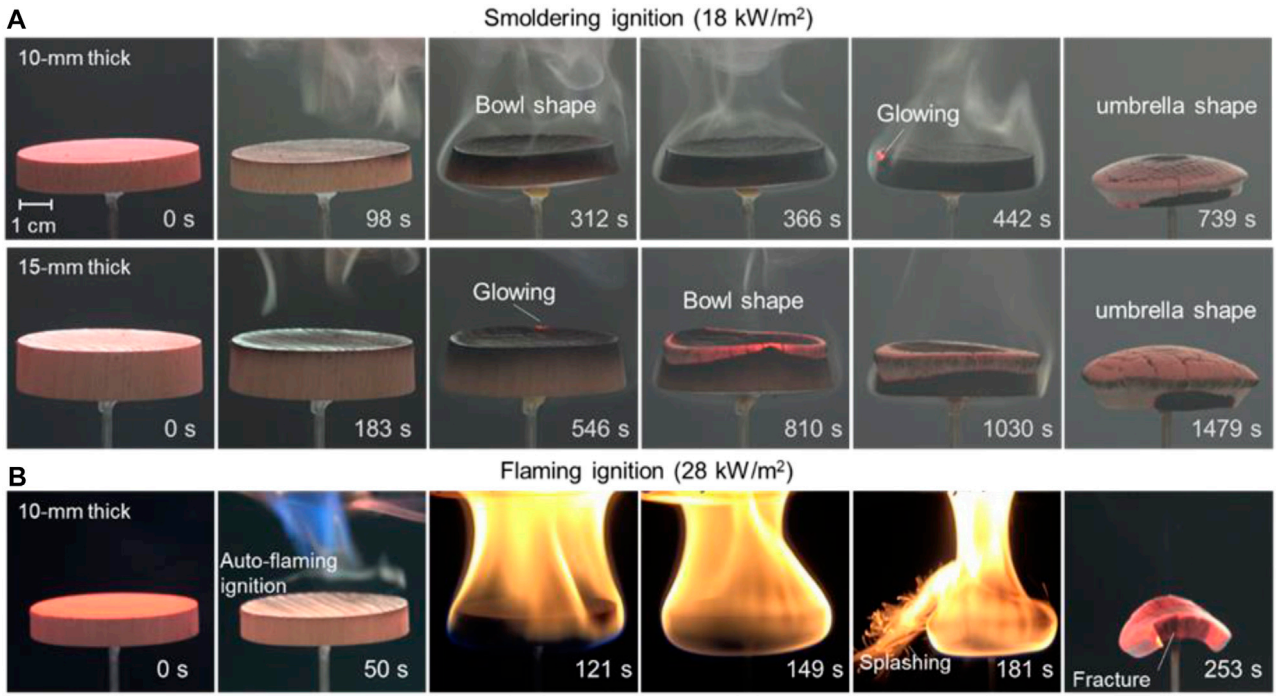

FIGURE 3 | (A) Smoldering ignition of the wood particle with a diameter of 60 mm and different thicknesses of 10 and 15 mm (Wang et al., 2021) and **(B)** flaming autoignition of the wood particle with a diameter of 60 mm and a thickness of 10 mm.

form a bowl shape. This may be caused by the shrinkage on the top surface, where there is a strong mass loss because of the drying and pyrolysis.

ii) Bending downward to form an umbrella shape. As the smoldering front approached the bottom, the sample bent back to become flat and then continued to bend downward and deformed to form an umbrella shape because of the interaction between thermal expansion and char oxidation (Wang et al., 2021).

Furthermore, a longer heating duration is required for a thicker sample to form a gas jet, as shown in **Figure 3A**. It was roughly attributed to the larger temperature gradients inside the thicker wood sample, and only the top thin layer can reach its pyrolysis temperature to release gases (Lin et al., 2019a). For the samples with thicknesses of 5 and 10 mm, the regression due to burnout on the top surface occurred after the smoldering front reached the bottom surface, whereas for the thickness of 15 mm, the regression occurred earlier. Therefore, we can presume that the characteristic thickness of the smoldering front is about 10–15 mm for this wood particle.

Flaming Autoignition and Burning Behaviors

The flaming autoignition of the wood particle was also observed as the external heat flux is larger than the critical value ($\dot{q}''_{min,f}$). **Figure 3B** shows an example of the flaming autoignition and burning processes of the large disc-shaped wood sample with a diameter of 60 mm and a thickness of 10 mm. The original video can be found in **Supplemental Video S3**. After heating for about 50 s, a blue flash could be achieved above the wood top surface. Subsequently, the flame propagated downward and covered the entire sample surface. At 253 s, the flame self-extinguished, and the wood residue was in an umbrella-shaped structure. However, the extinction of the flame is not the end of the fire; instead, it was followed by a stable smoldering in the solid phase until burnout (Lin et al., 2021). Compared with the smoldering burning of the 10-mm-thick sample in **Figure 3A**, the structure deformation and edge effect were not obvious during the flaming burning.

On the other hand, during the burning process, the macro-cracking occurred on the sample surfaces, which was widely observed in wood pyrolysis processes under the nitrogen condition (Li et al., 2017). Such cracking was due to the accumulation of internal pressure and structure failure. Moreover, the splashing phenomenon was also observed, which was a strong bright spark, like that occurs upon water dripping into boiling oil. Such a splash phenomenon might be the result of the competition of gas production and sample structural strength (see **Appendix** for more details).

The Ignition Limits of Flaming and Smoldering

By plotting the ignition time under different radiant heat fluxes, the propensity for flaming and smoldering ignition of the wood particle can be quantified. **Figure 4A** shows an example of a wood particle with a diameter of 60 mm and a thickness of 10 mm. The error bars show the standard deviations of the values measured from all repeating tests. As expected, the ignition delay time also decreases as radiant heat flux increases, the same as other

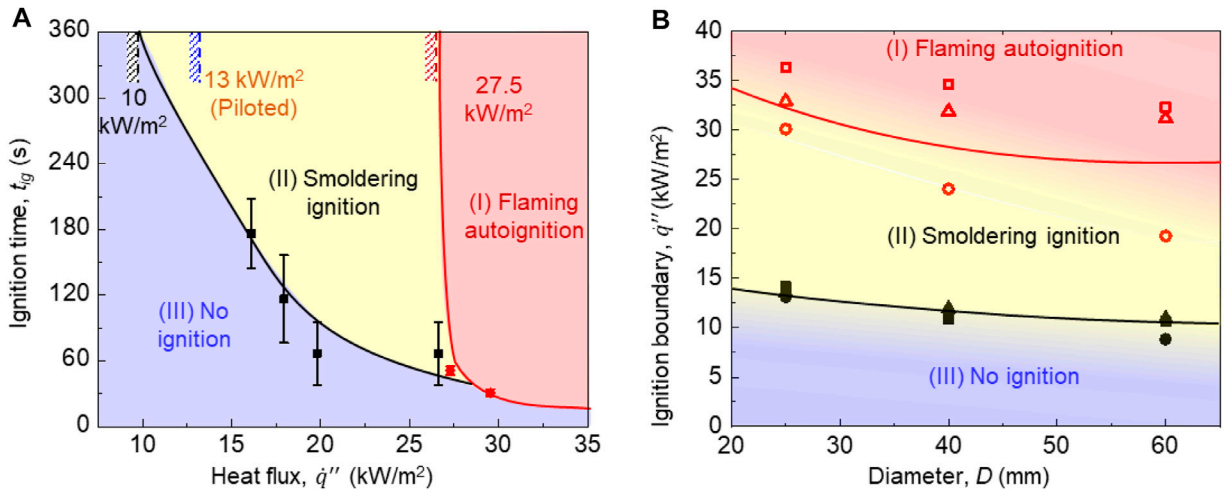

FIGURE 4 | (A) Smoldering ignition and flaming autoignition delay time of wood particles (D = 60 *mm*, δ = 10 *mm*) under different heat fluxes. **(B)** Effect of fuel size on the ignition boundary of the wood particle. The symbols of the square, triangle, and circle represent the thicknesses of 15, 10, and 5 mm, and the red and black symbols represent flaming and smoldering ignition, respectively. The striped regions represented the lowest heat fluxes or ignition boundary of smoldering ignition, piloted ignition, and autoignition, respectively.

combustibles (Rodriguez et al., 2017). More importantly, by decreasing the radiant heat flux and ignition time, the observed phenomena in the current non-piloted ignition study can be categorized into three regions: (I) flaming autoignition, (II) smoldering ignition, and (III) no ignition. A much larger heat flux is required to initiate the flaming ignition of wood particles in the absence of a pilot source than the smoldering ignition of wood particles (10 kW/m^2 vs. 28 kW/m^2), which is different from the ignition propensity of peat soil (6.5 kW/m^2 vs. 7.5 kW/m^2) (Lin et al., 2019b) with pilot source and the glowing autoignition of wood cubic samples (10 kW/m^2 vs. 18 kW/m^2) (Boonmee and Quintiere, 2002).

For comparison, the critical heat flux for the piloted ignition of wood from the study by Quintiere (2006) is also plotted in **Figure 4A**. Here, the striped regions represented the lowest heat fluxes or ignition boundaries of smoldering ignition, piloted ignition, and autoignition, respectively. The difficulty of ignition increases from smoldering to piloted flaming ignition and then to flaming autoignition in terms of the minimum heat flux. Therefore, the piloted ignition effectively lowers the flaming ignition limit and provides a shortcut to trigger a flaming fire. In real fire scenarios, the flame of burning trees can act as the heating and pilot sources, which may cause piloted flaming ignition and increase the wildfire risk.

Figure 4B further summarizes the ignition boundaries of smoldering ignition and flaming autoignition for different wood particles, where the symbols of the square, triangle, and circle represent the sample thicknesses of 15, 10, and 5 mm and the red and black symbols represent flaming and smoldering ignition, respectively. The ignition limit of flaming fire is very sensitive to the sample thickness, while the effect on smoldering ignition is negligible. For example, with the same diameter of 25 mm, as the same thickness increases from 5 to 15 mm, the critical heat flux for flaming ignition increases from 30 kW/m^2 to 37 kW/m^2. One possible reason is that for a thinner sample, both the received external radiation and the in-depth conduction are more uniform, leading to a smaller internal temperature gradient (Lin, Huang, et al., 2019). Therefore, a thicker layer below the top surface can reach pyrolysis temperature so that sufficient pyrolysis gases could be released to trigger flaming ignition. In contrast, for the sample with larger thickness, there is a large temperature gradient, and the in-depth temperature is much lower than the surface temperature. As a result, only the thin surface layer is pyrolyzing, so a larger external heat flux is required to reach the minimum fuel mass flux (Quintiere 2006) (discussed more in *Surface Temperature and Mass Loss Rate* in *Size Effect on the Flaming Burning Behaviors*). On the other hand, the minimum heat fluxes of both smoldering ignition and flaming autoignition are insensitive to the diameters, except the auto-flaming ignition of the 5-mm-thick sample, which has lower thermal resistance and is easily affected by the environmental factors.

Characteristics of Smoldering and Flaming Autoignition

Figure 5 shows an example of the measured surface temperature and mass-loss rates' time evolution for smoldering and flaming ignition of the wood particle with a thickness of 10 mm and a diameter of 60 mm. The red curves represent the flaming autoignition (28 kW/m^2), and the black curves represent the smoldering ignition (18 kW/m^2). Once exposed to the heating panel, both the surface temperature and mass loss increase remarkably with a decreasing rate. For flaming ignition, a sudden increase can be observed at the ignition moment in both surface temperature and mass flux, consistent with other research efforts (Moghtaderi et al., 1997; McAllister, 2013). For smoldering ignition, a sudden increase could also be observed in the mass flux, but it is not clear in the

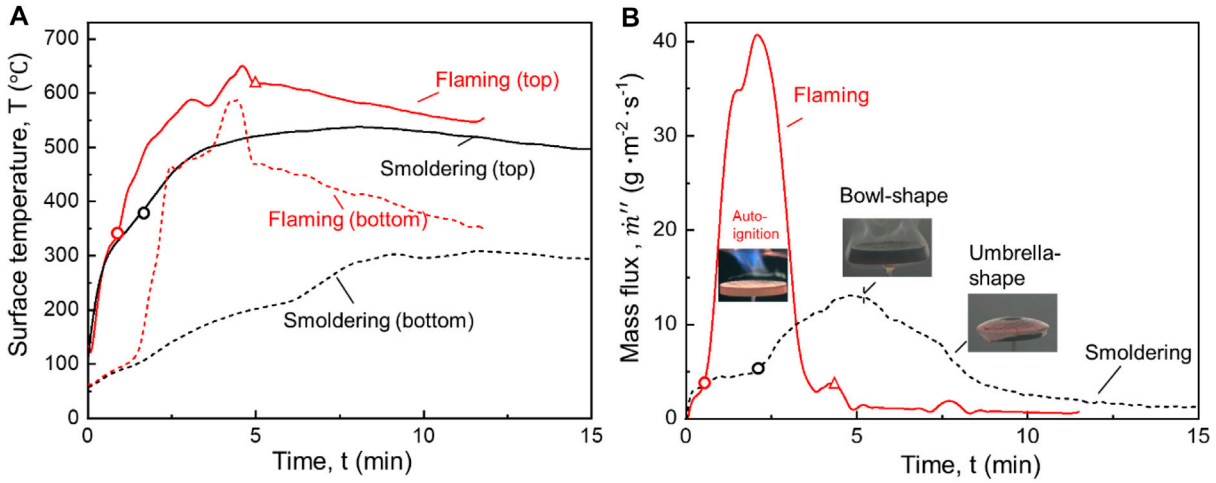

FIGURE 5 | Surface temperature **(A)** and mass loss time evolution **(B)** of the wood sample with a diameter of 60 mm and a thickness of 10 mm, where the circular symbols indicate the moment of flaming autoignition.

temperature evolution. However, the corresponding surface temperature at the smoldering ignition moment is found to be ~350°C, consistent with the findings of Terrei et al. (2019). Although the surface temperature during a flaming fire is much higher than that for a smoldering fire, their temperature difference between the top and bottom surfaces is smaller. Therefore, the thermal expansion for flaming fire is smaller than that for smoldering, as shown in **Figure 3**.

On the other hand, the mass flux for flaming is much higher than that for smoldering. For flaming burning, once the whole sample is charred, both the surface temperature and mass flux go through a sharp drop, following the self-extinction of flaming fire (Lin et al., 2021). However, the fire continues as smoldering combustion at very low mass flux, and the temperature difference keeps increasing and gradually becomes close to that of the direct smoldering ignition sample. For the flaming ignition criterion, ignition temperature (T_{ig}) is widely used, and it is very helpful in predicting the fire spread (Quintiere, 2006). If the external radiant heat flux is below the minimum value, an equilibrium between radiant heating and environmental cooling can be reached at a surface temperature below T_{ig} (Lin et al., 2019b).

Size Effect on the Flaming Burning Behaviors

Figure 6A plots the flaming ignition temperatures of wood samples with different diameters and thicknesses. It can be found that the flaming ignition temperature increases with the thickness, while it is less sensitive to the diameter. For example, for the wood particle with a diameter of 25 mm, the ignition temperature increases from 345 to 390°C as the sample thickness increases from 5 to 15 mm. Similarly, the temperature difference between the top and bottom surfaces at the ignition moment also increases with the sample thicknesses, as shown in **Figure 6B**.

A smaller temperature diffidence indicates a smaller internal temperature gradient in the direction perpendicular to the heating source, and both received external radiant heat flux and the in-depth conduction is more uniform (Lin et al., 2019a). Therefore, a thicker layer below the surface can reach the pyrolysis temperature and release combustible gases to trigger a flame. Comparatively, for the wood sample with a larger thickness, the in-depth temperature is much lower than the surface temperature, and only a very thin layer can reach the pyrolysis temperature, so a higher ignition temperature and the critical heat flux are required to reach the minimum fuel mass flux, as shown in **Figures 4B**, **6A**.

Figures 6C,D further compare the peak burning flux and flame duration of wood particles with different diameters and thicknesses. Clearly, as the thickness increases, the peak burning flux decreases while the flame duration increases. A thinner sample can burn more extensively due to a more uniform in-depth conduction so that it is easier for the whole sample to reach its pyrolysis temperature and start to burn.

Size Effect on Smoldering Burning Behaviors

Figure 7 and **Figure 8** present the thickness effect on the surface temperature and mass loss for smoldering combustion of samples with the same diameter of 60 mm. At about 35 s, the thermal energy had propagated to the lower face, and the pyrolysis gas was released. So, the small peak mass occurred at the initial heating only for the 5-mm-thick sample. Based on the characteristic temperature in TGA, the onset of "pyrolysis" and the onset of the "oxidation reaction" were determined. For sample thicknesses of 5, 10, and 15 mm, the onset of pyrolysis was at 54 ± 2, 69.5 ± 1.5, and 86 ± 4 s and the onset of the oxidation reaction was at 112 ± 5, 130.5 ± 2.5, and 143.5 ± 6.5 s, respectively. The thicker

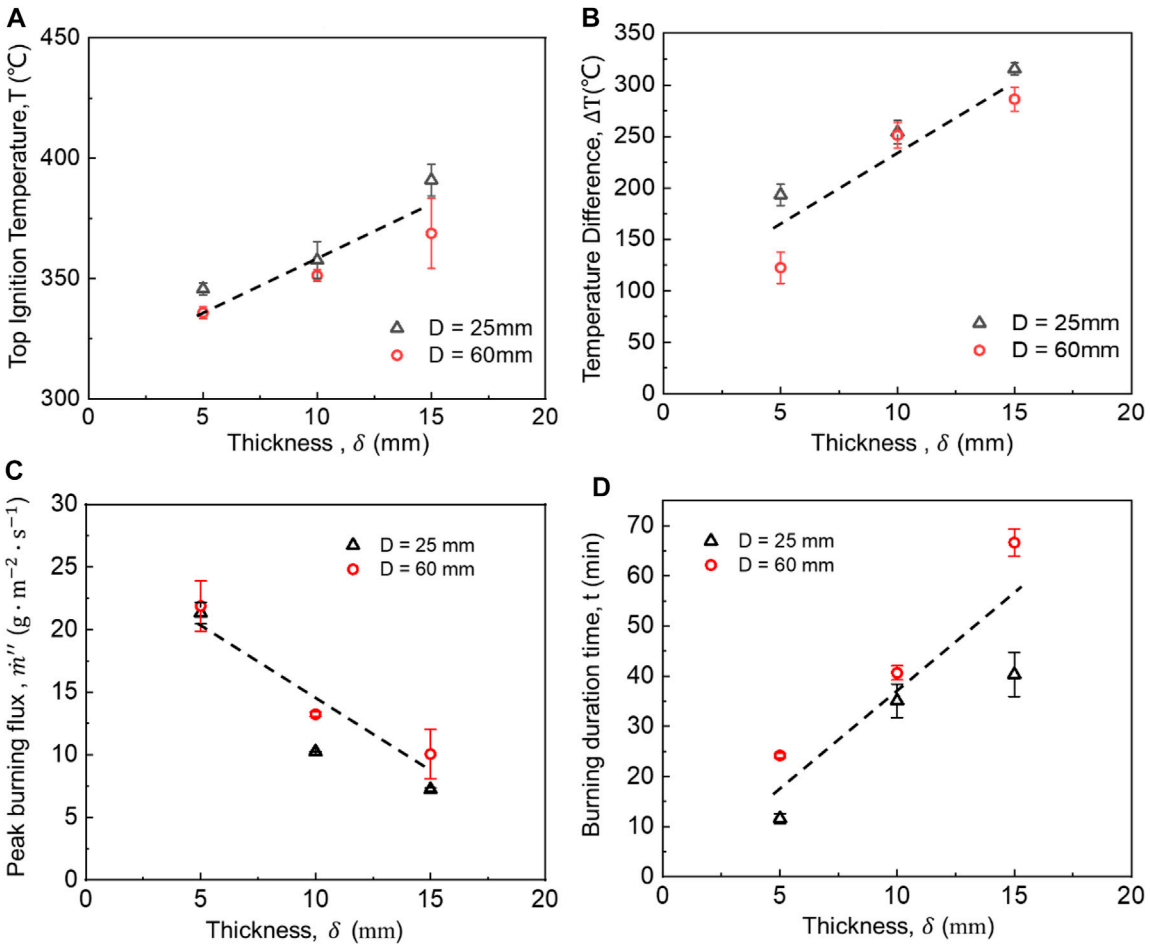

FIGURE 6 | Comparison of **(A)** autoignition fuel temperature, **(B)** temperature difference between the top and bottom surfaces at the ignition moment, **(C)** peak burning flux, and **(D)** burning duration time of flaming fire with different diameters and thicknesses.

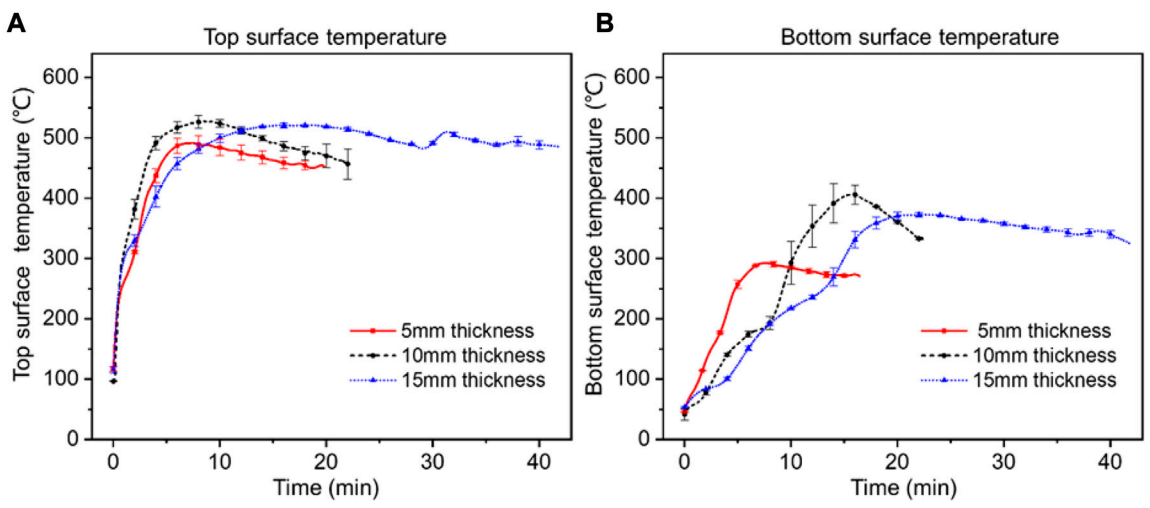

FIGURE 7 | Upper **(A)** and lower **(B)** face temperature during the smoldering ignition and burning for disc-shaped wood particles with a diameter of 60 mm, showing the thickness effect.

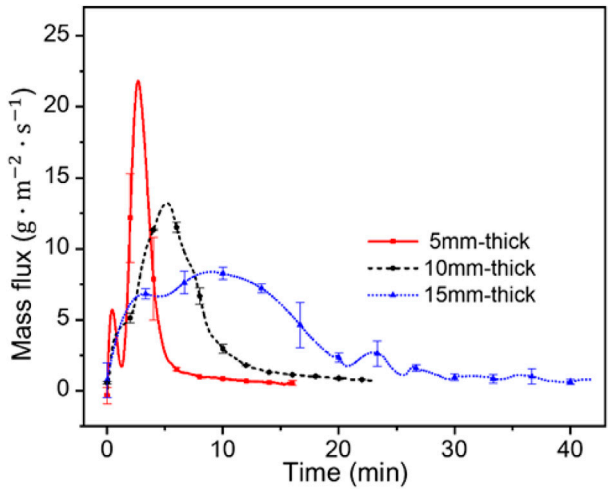

FIGURE 8 | Mass loss rate during the smoldering ignition and burning of disc-shaped wood particles with a diameter of 60 mm, showing the thickness effect.

particle has greater in-depth heat conduction, which delayed the appearance of pyrolysis and oxidation and decreased the peak reaction intensity, as indicated by the peak mass loss rate.

Due to the volume of the reaction fuel, the thickness had no obvious effect on the magnitude of upper face temperature. Conversely, the increment of thickness delayed and reduced the heating of the lower face. Also, there was one mass loss peak for $\delta < 10$ mm and two mass loss peaks for $\delta > 10$ mm. It was because the heating of the upper sample to pyrolysis of the unreacted materials is consistent with the oxidation phenomena in **Figure 2A**.

Figure 9 presents the diameter effect on the surface temperature and mass loss for smoldering combustion of 10-mm-thick samples. For the sample with the diameters of 25 and 60 mm, the onset of pyrolysis was at 62.5 ± 1.5 and 69.5 ± 1.5 s, and the onset of the oxidation reaction was at 102 ± 1 and 130.5 ± 2.5 s, respectively. Despite the same upper face temperature before 15 s, the accumulation of heat on the side surface accelerated the temperature increase of the lower face and also moved up the appearance of the smoldering onset for the sample with a diameter of 25 mm compared to that for the sample with a diameter of 60 mm. Until the onset of the oxidation of the sample with a diameter of 60 mm, its lower face temperature was higher than that of the sample with a diameter of 25 mm. Because of the difference of latent heat release, the lower face temperature of the sample with a diameter of 25 mm was lower than that of the sample with a diameter of 60 mm. The diameter had no effect on the peak temperature of the upper face temperature. There was the shoulder peak for the mass loss rate for the sample with a diameter of 25 mm, which was different from the single peak for the sample with a diameter of 60 mm. The shoulder might be attributed to the sequential oxidation reaction of both sides and the heating of the oxidation reaction for the entire sample.

Figure 10 presents the thickness and diameter effect on smoldering characteristic values for samples with a diameter of 60 mm. The increment of the size (both thickness and diameter) held the lower peak burning rate and the larger burning duration time. Thus, smoldering ignition should be significantly more sensitive to sample thickness than to sample diameter in the size range studied.

CONCLUSION

In this experimental work, we found that the ignition difficulty of the stationary disc-shaped wood particle increases from smoldering ignition to piloted flaming

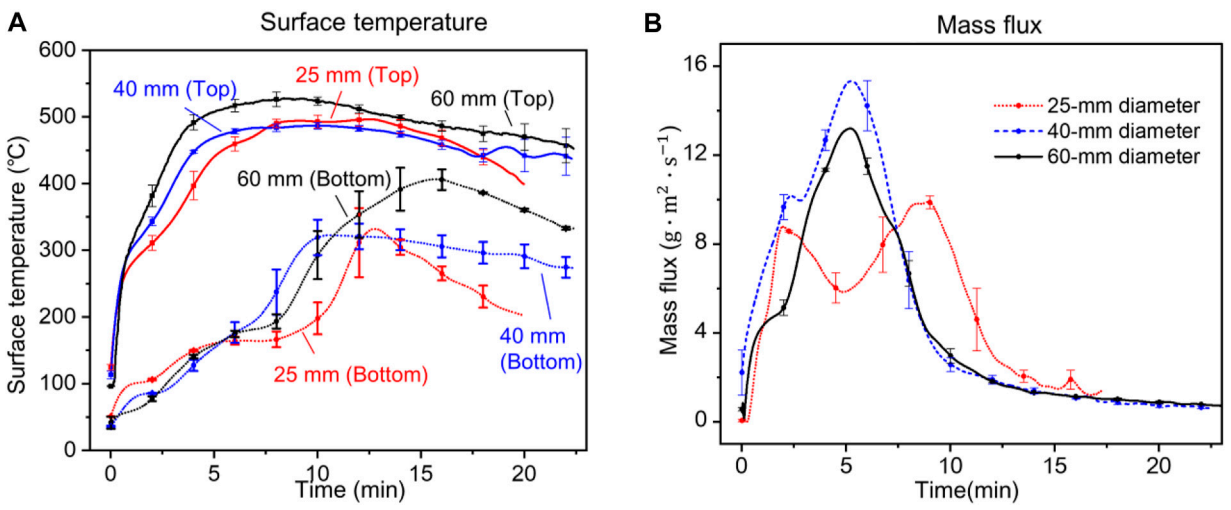

FIGURE 9 | Surface [upper (U) and lower (L)] temperature **(A)** and mass flux **(B)** vs. time: diameter effect on smoldering combustion for 10-mm-thick samples.

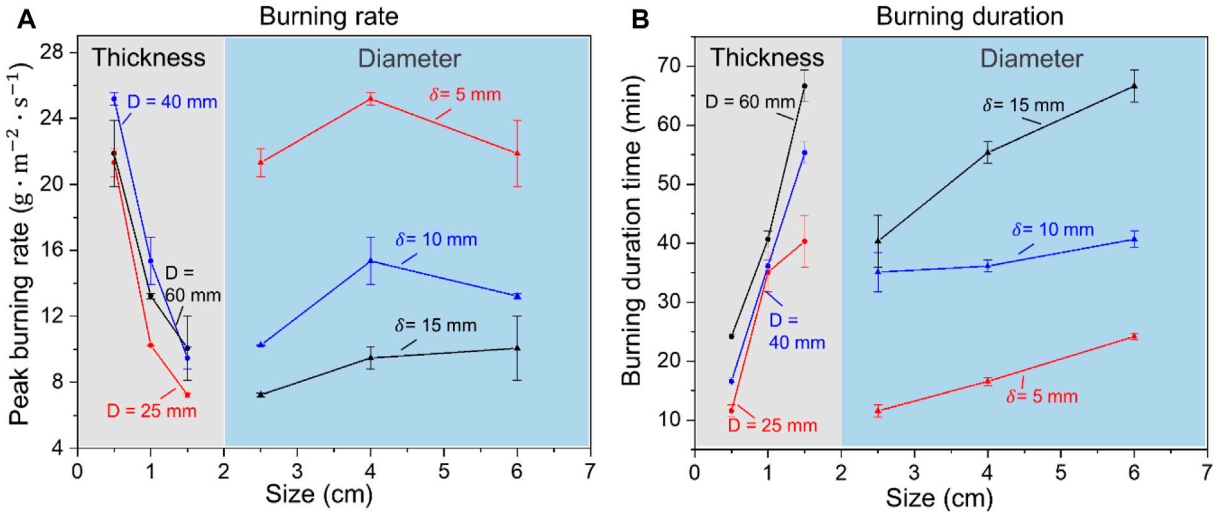

FIGURE 10 | Summarized size (thickness and diameter) effect on smoldering characteristics: **(A)** peak mass flux and **(B)** burning duration or burnout time.

ignition and then to flaming autoignition, as the required minimum heat flux approximately increases from 10 kW/m^2 to 30 kW/m^2. Compared to the smoldering ignition, the flaming autoignition is very sensitive to the fuel thickness (5–15 mm), while the effect of diameter (25–60 mm) is negligible. The ignition temperature, minimum heat flux, and burning duration of flaming all increase, while the peak burning flux decreases, as the wood thickness increases.

During the ignition and the following burning processes, the disc-shaped particle was first deformed to a bowl shape and then to an umbrella shape due to the interaction between chemical reactions and thermomechanical stresses. The characteristic thickness of the smoldering front on wood is also found to be 10–15 mm. This study helps understand the interaction between flaming and smoldering wildfires and the deformation behaviors of the wood particles in wildfires. In our future work, numerical simulations will be conducted to reproduce the deformation behaviors of wood particles and improve the up-to-date pyrolysis modeling technology.

DATA AVAILABILITY STATEMENT

The raw data supporting the conclusions of this article will be made available by the authors, without undue reservation.

AUTHOR CONTRIBUTIONS

SW: conceptualization, methodology, writing—original draft, formal analysis, and funding acquisition. PD: investigation, resources, and writing—original draft. SL: investigation, writing—review and editing, and formal analysis. JG: investigation and resources. XH: methodology, formal analysis, supervision, and writing—review and editing.

FUNDING

This work is supported by the National Natural Science Foundation of China (NSFC nos. 51706095, 51974164, and 51876183), the Natural Science Foundation of Jiangsu Province of China (Grant no. BK20171001), the HK PolyU Postdoctoral Fellowship (Grant no. P0014039) and RISUD Emerging Frontier Area (EFA) Scheme (P0013879), and the China Postdoctoral Science Foundation (Grant no. 2017M611798).

SUPPLEMENTARY MATERIAL

The Supplementary Material for this article can be found online at: https://www.frontiersin.org/articles/10.3389/fmech.2021.686638/full#supplementary-material

REFERENCES

Atreya, A., Olszewski, P., Chen, Y., and Baum, H. R. (2017). The Effect of Size, Shape and Pyrolysis Conditions on the thermal Decomposition of wood Particles and Firebrands. *Int. J. Heat Mass Transfer* 107, 319–328. doi:10.1016/j.ijheatmasstransfer.2016.11.051

Bilbao, R., Mastral, J. F., Aldea, M. E., Ceamanos, J., Betrán, M., and Lana, J. A. (2001). Experimental and Theoretical Study of the Ignition and Smoldering of wood Including Convective Effects. *Combustion and Flame*. 126, 1363–1372. doi:10.1016/S0010-2180(01)00251-6

Boonmee, N., and Quintiere, J. G. (2002). Glowing and Flaming Autoignition of wood. *Proc. Combustion Inst.* 29, 289–296. doi:10.1016/S1540-7489(02)80039-6

Finney, M. A., Cohen, J. D., Forthofer, J. M., McAllister, S. S., Gollner, M. J., Gorham, D. J., et al. (2015). Role of Buoyant Flame Dynamics in Wildfire Spread. *Proc. Natl. Acad. Sci. USA*. 112, 9833–9838. doi:10.1073/pnas.1504498112

Finney, M. A., Cohen, J. D., McAllister, S. S., and Jolly, W. M. (2013). On the Need for a Theory of Wildland Fire Spread. *Int. J. Wildland Fire*. 22 (2013), 25–36. doi:10.1071/WF11117

Harada, T. (2001). Time to Ignition, Heat Release Rate and Fire Endurance Time of wood in Cone Calorimeter Test. *Fire Mater.* 25, 161–167. doi:10.1002/fam.766

Huang, X., and Gao, J. (2021). A Review of Near-Limit Opposed Fire Spread. *Fire Saf. J.* 120, 103141. doi:10.1016/j.firesaf.2020.103141

Huang, X., and Rein, G. (2017). Downward Spread of Smouldering Peat Fire: the Role of Moisture, Density and Oxygen Supply. *Int. J. Wildland Fire*. 26, 907–918. doi:10.1071/WF16198

Incropera, F. P., and DeWitt, D. P. (1996). *Fundamentals of Heat and Mass Transfer*. John Wiley, New York. doi:10.1016/j.applthermaleng.2011.03.022

Kuo, J. T., and Hsi, C.-L. (2005). Pyrolysis and Ignition of Single Wooden Spheres Heated in High-Temperature Streams of Air. *Combustion and Flame*. 142, 401–412. doi:10.1016/j.combustflame.2005.04.002

Li, K., Hostikka, S., Dai, P., Li, Y., Zhang, H., and Ji, J. (2017). Charring Shrinkage and Cracking of Fir during Pyrolysis in an Inert Atmosphere and at Different Ambient Pressures. *Proc. Combustion Inst.* 36, 3185–3194. doi:10.1016/j.proci.2016.07.001

Lin, S., Huang, X., Gao, J., and Ji, J. (2021). Extinction of Wood Fire: A Near-Limit Blue Flame Above Hot Smoldering Surface. *Fire Technol.* doi:10.1007/s10694-021-01146-6

Lin, S., Huang, X., Urban, J., McAllister, S., and Fernandez-Pello, C. (2019a). Piloted Ignition of Cylindrical Widlland Fuels under Irradiation. *Front. Mech. Eng.* 5, 54. doi:10.3389/fmech.2019.00054

Lin, S., Sun, P., and Huang, X. (2019b). Can Peat Soil Support a Flaming Wildfire?. *Int. J. Wildland Fire*. 28, 601–613. doi:10.1071/WF19018

Liu, Y., Stanturf, J., and Goodrick, S. (2010). Trends in Global Wildfire Potential in a Changing Climate. *For. Ecol. Manage.* 259, 685–697. doi:10.1016/j.foreco.2009.09.002

Manzello, S. L., Cleary, T. G., Shields, J. R., Maranghides, A., Mell, W., and Yang, J. C. (2008). Experimental Investigation of Firebrands: Generation and Ignition of Fuel Beds. *Fire Saf. J.* 43, 226–233. doi:10.1016/j.firesaf.2006.06.010

Manzello, S. L., Suzuki, S., Gollner, M. J., and Fernandez-Pello, A. C. (2020). Role of Firebrand Combustion in Large Outdoor Fire Spread. *Prog. Energ. Combustion Sci.* 76, 100801. doi:10.1016/j.pecs.2019.100801

McAllister, S. (2013). Critical Mass Flux for Flaming Ignition of Wet wood. *Fire Saf. J.* 61, 200–206. doi:10.1016/j.firesaf.2013.09.002

Mcallister, S., and Finney, M. (2017). Autoignition of wood under Combined Convective and Radiative Heating. *Proc. Combustion Inst.* 36, 3073–3080. doi:10.1016/j.proci.2016.06.110

McAllister, S., Grenfell, I., Hadlow, a., Jolly, W. M., Finney, M., and Cohen, J. (2012). Piloted Ignition of Live forest Fuels. *Fire Saf. J.* 51, 133–142. doi:10.1016/j.firesaf.2012.04.001

Moghtaderi, B., Novozhilov, V., Fletcher, D. F., and Kent, J. H. (1997). A New Correlation for Bench-Scale Piloted Ignition Data of Wood. *Fire Saf. J.* 29, 41–59. doi:10.1016/S0379-7112(97)00004-0

Momeni, M., Yin, C., Knudsen Kær, S., and Hvid, S. L. (2013). Comprehensive Study of Ignition and Combustion of Single Wooden Particles. *Energy Fuels*. 27, 1061–1072. doi:10.1021/ef302153f

Moritz, M. A., Batllori, E., Bradstock, R. A., Gill, A. M., Handmer, J., Hessburg, P. F., et al. (2014). Learning to Coexist with Wildfire. *Nature* 515, 58–66. doi:10.1038/nature13946

Paulrud, S., and Nilsson, C. (2004). The Effects of Particle Characteristics on Emissions from Burning wood Fuel Powder. *Fuel* 83, 813–821. doi:10.1016/j.fuel.2003.10.010

Quintiere, J. G. (2006). *Fundamental of Fire Phenomena*. New York: John Wiley. doi:10.1002/0470091150

Rein, G. (2016). Smoldering Combustion. *SFPE Handbook Fire Prot. Eng.* 2014, 581–603. doi:10.1007/978-1-4939-2565-0_19

Rodriguez, A., Huang, X., Link, S., Olson, S., Ferkul, P., and Fernandez-pello, C. (2017). Piloted Ignition of Cylindrical PMMA and Wood. In 12th International Symposium on Fire Safety Science, June 17, 2017, Sweden, 36, 3073.

Rothermel, R. C. (1972). *A Mathematical Model for Predicting Fire Spread in Wildland Fuels*. Intermountain Forest & Range Experiment Station, Forest Service, U.S. Department of Agriculture, Logan, Utah.

Saastamoinen, J. J., Taipale, R., Horttanainen, M., and Sarkomaa, P. (2000). Propagation of the Ignition Front in Beds of wood Particles. *Combust. Flame*. 123, 214–226. doi:10.1016/S0010-2180(00)00144-9

Santoso, M. A., Christensen, E. G., Yang, J., and Rein, G. (2019). Review of the Transition from Smouldering to Flaming Combustion in Wildfires. *Front. Mech. Eng.* 5. 49. doi:10.3389/fmech.2019.00049

Simms, D. L., and Law, M. (1967). The Ignition of Wet and Dry wood by Radiation. *Combust. Flame* 11, 377–388. doi:10.1016/0010-2180(67)90058-2

Sullivan, A. L., Surawski, N. C., Crawford, D., Hurley, R. J., Volkova, L., Weston, C. J., et al. (2018). Effect of Woody Debris on the Rate of Spread of Surface Fires in forest Fuels in a Combustion Wind Tunnel. *For. Ecol. Manage.* 424, 236–245. doi:10.1016/j.foreco.2018.04.039

Terrei, L., Acem, Z., Georges, V., Lardet, P., Boulet, P., and Parent, G. (2019). Experimental Tools Applied to Ignition Study of spruce wood under Cone Calorimeter. *Fire Saf. J.* 108, 102845. doi:10.1016/j.firesaf.2019.102845

Toledo, T., Marom, I., Grimberg, E., and Bekhor, S. (2018). Analysis of Evacuation Behavior in a Wildfire Event. *Int. J. Disaster Risk Reduction* 31, 1366–1373. doi:10.1016/j.ijdrr.2018.03.033

Wang, H., van Eyk, P. J., Medwell, P. R., Birzer, C. H., Tian, Z. F., and Possell, M. (2016). Identification and Quantitative Analysis of Smoldering and Flaming Combustion of Radiata Pine. *Energy Fuels* 30, 7666–7677. doi:10.1021/acs.energyfuels.6b00314

Wang, H., van Eyk, P. J., Medwell, P. R., Birzer, C. H., Tian, Z. F., Possell, M., et al. (2017a). Effects of Oxygen Concentration on Radiation-Aided and Self-Sustained Smoldering Combustion of Radiata Pine. *Fire Saf. J.* 31, 427–443. doi:10.1016/j.firesaf.2006.03.006

Wang, S., Huang, X., Chen, H., and Liu, N. (2017b). Interaction between Flaming and Smouldering in Hot-Particle Ignition of forest Fuels and Effects of Moisture and Wind. *Int. J. Wildland Fire* 26, 71–81. doi:10.1071/WF16096

Wang, S., Ding, P., Lin, S., Huang, X., and Usmani, A. (2021). Deformation of wood Slice in Fire: Interactions between Heterogeneous Chemistry and Thermomechanical Stress. *Proc. Combust. Inst.* 38, 5081–5090. doi:10.1016/j.proci.2020.08.060

Wesson, H. R., Welker, J. R., and Sliepcevich, C. M. (1971). The Piloted Ignition of wood by thermal Radiation. *Combust. Flame* 16, 303–310. doi:10.1016/S0010-2180(71)80101-3

Williams, F. A. (1982). Urban and Wildland Fire Phenomenology. *Prog. Energ. Combust. Sci.* 8, 317–354. doi:10.1016/0360-1285(82)90004-1

Yang, L., Zhou, Y., Wang, Y., Dai, J., Deng, Z., and Zhou, X. (2011). Autoignition of Solid Combustibles Subjected to a Uniform Incident Heat Flux: The Effect of Distance from the Radiation Source. *Combust. Flame*. 158, 1015–1017. doi:10.1016/j.combustflame.2011.01.008

Conflict of Interest: The authors declare that the research was conducted in the absence of any commercial or financial relationships that could be construed as a potential conflict of interest.

APPENDIX

A high-speed camera was used to trace the splash phenomenon for the sample with a diameter of 60 mm and a thickness of 10 mm, and the result is shown in **Figure A1**. The original video can be found in **Supplementary Video S4**. Here, the starting point (i.e., 0 ms) was set at the moment that the record was started. The crack occurred at 72 ms on the sample surface, and splashing occurred with the tiny particles quickly flying out from the fracture at 102 ms. The splashing phenomena would be sustained for hundreds of milliseconds. During this time, there was also the dropping of the ember from the sample at 144 ms and generating many small embers nearby.

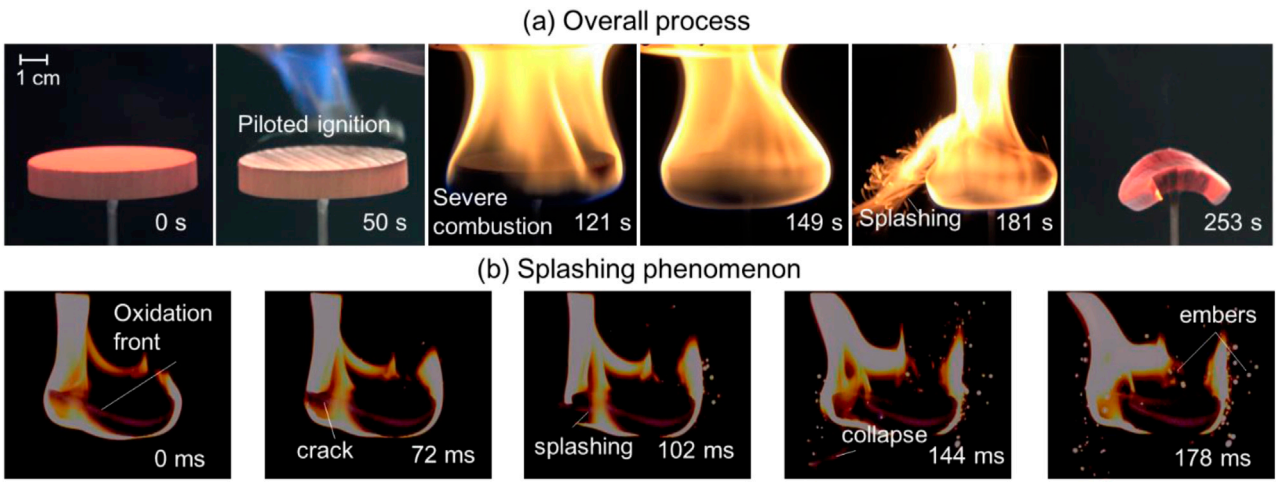

FIGURE A1 | Example of **(A)** overall flaming ignition and burning process and **(B)** splashing process is traced using a high-speed camera at 500 fps of the disc diameter of 60 mm and the disc thickness of 10 mm (**Supplementary Video S4**).